PAPER • **OPEN ACCESS**

Photocatalytic degradation of methylene blue at nanostructured ZnO thin films

To cite this article: Anna Kulis-Kapuscinska *et al* 2023 *Nanotechnology* **34** 155702

OPEN ACCESS
IOP Publishing
Nanotechnology

Nanotechnology **34** (2023) 155702 (11pp) https://doi.org/10.1088/1361-6528/aca910

Photocatalytic degradation of methylene blue at nanostructured ZnO thin films

Anna Kulis-Kapuscinska[1], Monika Kwoka[1,*], Michal Adam Borysiewicz[2], Tomasz Wojciechowski[3], Nadia Licciardello[4,6], Massimo Sgarzi[5,*] and Gianaurelio Cuniberti[4,*]

[1] Department of Cybernetics, Nanotechnology and Data Processing, Faculty of Automatic Control, Electronics and Computer Science, Silesian University of Technology, Akademicka 16, 44-100 Gliwice, Poland
[2] Łukasiewicz Research Network—Institute of Microelectronics and Photonics, Aleja Lotników 32/46, 02-668 Warsaw, Poland
[3] International Research Centre MagTop, Institute of Physics, Polish Academy of Sciences, Aleja Lotników 32/46, 02-668 Warsaw, Poland
[4] Institute for Materials Science, Max Bergmann Centre of Biomaterials and Dresden Center for Nanoanalysis, TU Dresden, D-01062, Dresden, Germany
[5] Department of Molecular Sciences and Nanosystems, Ca' Foscari University of Venice, Via Torino 155, I-30172 Venezia Mestre, Italymonika.kwoka@polsl.pl, massimo.sgarzi@unive.it and gianaurelio.cuniberti@tu-dresden.de

Received 16 June 2022, revised 20 November 2022
Accepted for publication 6 December 2022
Published 30 January 2023

Abstract

The photocatalytic degradation of the wastewater dye pollutant methylene blue (MB) at ZnO nanostructured porous thin films, deposited by direct current reactive magnetron sputtering on Si substrates, was studied. It was observed that over 4 photocatalytic cycles (0.3 mg $\cdot$ l^{-1} MB solution, 540 minUV irradiation), the rate constant k of MB degradation decreased by ~50%, varying in the range $(1.54 \div 0.78) \cdot 10^{-9}$ (mol·l^{-1}·min^{-1}). For a deeper analysis of the photodegradation mechanism, detailed information on the nanostructured ZnO surface morphology and local surface and subsurface chemistry (nonstoichiometry) were obtained by using scanning electron microscopy (SEM) and x-ray photoelectron spectroscopy (XPS) as complementary analytical methods. The SEM studies revealed that at the surface of the nanostructured ZnO thin films a coral reef structure containing polycrystalline coral dendrites is present, and that, after the photocatalytic experiments, the sizes of individual crystallites increased, varying in the range 43 ÷ 76 nm for the longer axis, and in the range 28 ÷ 58 nm for the shorter axis. In turn, the XPS studies showed a slight non-stoichiometry, mainly defined by the relative [O]/[Zn] concentration of ca. 1.4, whereas [C]/[Zn] was ca. 1.2, both before and after the photocatalytic experiments. This phenomenon was directly related to the presence of superficial ZnO lattice oxygen atoms that can participate in the oxidation of the adsorbed MB molecules, as well as to the presence of surface hydroxyl groups acting as hole-acceptors to produce OH· radicals, which can be responsible for the generation of superoxide ions. In addition, after experiments, the XPS measurements revealed the presence of carboxyl and carbonyl functional groups, ascribable to the oxidation by-products formed during the photodegradation of MB.

[6] Current Address: Department of Drug and Health Sciences, University of Catania, Viale Andrea Doria 6, 95125 Catania.
[*] Authors to whom any correspondence should be addressed.

Keywords: methylene blue, photocatalytic degradation, ZnO thin films nanostructures, immobilized photocatalysts

1. Introduction

In recent years, due to population growth and worldwide industrial development, the contamination of surface and groundwater has quickly increased. One of the main sources of surface and groundwater contamination is organic dyes: due to their high toxicity together with their nonbiodegradability, they cause not only several environmental hazards but also health-related issues [1].

In this context, one of the main research challenges is the removal of hazardous dyes from wastewater by using treatments that do not present a serious undesired impact on the environment on one hand, and are relatively simple and not too expensive, on the other hand. One of the most common hazardous dyes in wastewater is methylene blue (tetramethylthionine chloride, MB; for chemical structure, refer to figure S1), which is used, among different fields, in the textile industry, as a dye for wool, silk, leather and cotton [2]. However, during the dyeing process, a large portion (up to 15%) [3] is normally transferred into the wastewater. Unfortunately, MB can directly retard the biological activity of various aquatic plants and animals including fishes and other organisms in the surrounding environment [4].

So far, various methodologies have been implemented for wastewater treatment to remove hazardous dyes by using different approaches, which can be divided into two groups, i.e. separation methods, which can include physical and physico-chemical means, and degradation methods, in which biological and chemical processes are involved, as reviewed by Nidheesh *et al* [5]. Among the separation methods, one can distinguish adsorption processes based on solid adsorbents [6, 7], coagulation and flotation [8], and membrane filtration [9]. In turn, within the group of degradation methods, one can distinguish several methods such as, just to cite a few, biodegradation [10], chemical catalytic reactions combined with biological oxidations [11], and advanced oxidation processes (AOPs) [12, 13]. Most of the mentioned techniques are associated with various drawbacks, such as the production of toxic by-products, high costs, limited recovery, or high energy consumption [14]. Out of the AOPs, photocatalysis, which makes use of semiconductor oxide photocatalysts to perform pollutant photodegradation in wastewater [14, 15], is widely used because it can reduce the concentration of hazardous organic compounds in water. In general, the photocatalytic method consists of the light-activated (UV or visible radiation) production of radical species able to oxidize the pollutants dissolved in water. The entire process can be schematized in the following six steps (see figure 1.): (i) the photocatalyst is activated via the absorption of light, which induces the formation of electron–hole pairs. In turn, these react with water and oxygen dissolved in water to produce reactive oxygen species such as superoxide ions (O_2^-) and hydroxyl radicals (OH·); (ii) the organic pollutant diffuses from the liquid phase to the surface of the photocatalyst, where (iii) it is adsorbed; (iv) the photocatalytic reaction between the adsorbate and the radical species takes place; (v) the products of the photocatalytic reaction are desorbed, and subsequently (vi) they diffuse away from the photocatalyst surface.

Heterogeneous photocatalysis has been proved as a promising method for the degradation of organic pollutants contained in wastewater. The process, as a means of removal of persistent water contaminants such as dyes, pharmaceuticals, and pesticides, has attracted the attention of many researchers in recent years [16–19].

The main advantage of photocatalysis is related to the fact that ideally, after the pollutant degradation, harmless final products such as CO_2, H_2O, and inorganic salts are obtained. This aspect is extremely important with regard to the undesired potential impact of photocatalysis on the environment [20].

Among the photocatalytic functional materials [21], mainly oxide semiconductors including titanium oxide (TiO_2) and zinc oxide (ZnO) have received much attention in the last decades as photocatalysts for the photodegradation of organic pollutants [22–27], due to their easy availability, low-toxicity, thermal and chemical stability [28–30].

Zinc oxide (ZnO) has been used on a large scale as an effective, inexpensive semiconductor photocatalyst for the degradation of a wide range of organic chemicals [31–33].

Moreover, it is common knowledge that ZnO is more efficient than TiO_2 for the degradation of water pollutants, despite the fact that both photocatalysts present a similar band gap energy (i.e. ∼3.2 eV) [34]. This is related to the fact that ZnO exhibits a large room temperature exciton (photoinduced electron–hole pairs) binding energy of 60 meV, a high electrical conductivity ($\sim 10^2\ \Omega^{-1}\cdot cm^{-1}$), and lower electric potentials of the valence and conduction bands (−0.45 to 2.75 eV, respectively) in comparison to TiO_2 (−0.1 to 3.1 eV, respectively). All these properties can explain why, for ZnO, more effective photocatalytic degradation reactions are observed at lower band potentials [35, 36].

It should be underlined that the ZnO band gap limits its photocatalytic activity mainly to the UV region (only 3%–4% of solar light). In order to extend its photocatalytic activity also in the visible region (∼44% of solar light) [36], one strategy is the modification of ZnO morphology to obtain various forms of ZnO nanostructures at the micro- and nanoscale, which provide also more active sites for the photocatalytic reactions [37, 38].

As a general trend, the size of the crystallites has a primary influence on ZnO photocatalytic activity: nanometre-scale crystallites exhibit better performance than submicron ones, which in turn outperform micron-scale ones [39]. This behavior can be explained in terms of specific surface area, which is higher for nanoscale materials, providing a higher number of active sites. On the other hand, the increase of defect concentration induced by the size decrease favors

electron–hole recombination processes, resulting in low photocatalytic activities of ultrasmall nanocrystallites [40–44]. An optimum crystallite size that maximises the photocatalytic activity is thus generally observed. As far as morphology is concerned, recent studies indicate that the ZnO (0 0 1) facet accelerates the production of OH· radicals, which are one of the active species responsible for the photocatalytic degradation of dyes [43].

Altogether, in the last years, much work has been done to explore the photocatalytic activity of several specific ZnO low-dimensional nanostructures, which were reviewed in the recent literature [14, 15, 44–51].

Among the ZnO two-dimensional nanostructures used as photocatalysts, apart from nanoparticles [52–54] and nanopowders [55], mainly ZnO thin films are preferred for photocatalytic applications: their use can facilitate the photocatalyst separation process, and the recycling and regeneration steps, which can be cumbersome with non-supported photocatalysts. These thin films are usually prepared by different deposition methods, such as magnetron sputtering [56, 57], spray pyrolysis [58, 59], sol-gel process [60, 61], as well as combined sonochemical and hydrothermal deposition.

In turn, among the ZnO one-dimensional nanostructures, mostly the crystalline nanoforms are preferred as visible light photocatalysts, including nanowires [62, 63], nanorods [64, 65], as well as the hierarchical ZnO nanoforms [62–64], such as nanoflowers [43, 65–67], and nanosheets [68–70].

Despite the great amount of dedicated research, the mechanism of the photocatalytic degradation of dyes using the various forms of low dimensional ZnO nanostructures remains mostly unknown [71–73]. This is probably related to the fact that the techniques commonly used for the characterization of these nanomaterials such as XRD and SEM are not fully surface-sensitive in character.

To achieve efficient photocatalytic degradation, efficient adsorption at the photocatalyst surface is fundamental. This is because adsorption processes take place at the surface and within the subsurface region of semiconductor photocatalysts. These processes directly cause a charge redistribution within the surface space-charge region related to Debye length L_D, and induce a surface band bending effect playing a crucial role in the specific surface conduction mechanism. This effect is also observed in the various nanoforms of ZnO, for which the carrier concentration reaches the value of $\sim 10^{18}$ [cm^{-3}], and usually, a surface depletion region with common upward band bending is observed at the depth of 1 nm [74]. Thus, it is evident that, apart from the information concerning the local surface crystallinity and morphology, the detailed information on local surface and subsurface chemistry of the selected low dimensional ZnO nanostructures, including mainly their stoichiometry (combined with the undesired surface contaminants), should be also taken into account for a deeper analysis of the mechanism of photocatalytic degradation of pollutants at their surface.

For this purpose, one of the best methods is x-ray photoemission spectroscopy (XPS), whose information depth is comparable to the Debye length L_D. This method has been successfully used for the study, among others, of the surface chemistry of the nanostructured ZnO porous thin films [74, 75], exhibiting the highest extension of the specific internal surface of ZnO thin films.

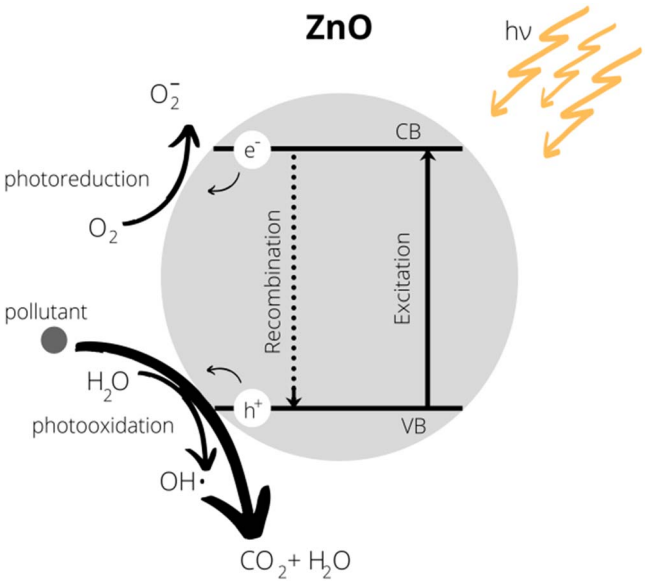

Figure 1. Mechanism of the photocatalytic degradation of pollutants in the presence of a ZnO photocatalyst.

Here, we propose an x-ray photoelectron spectroscopy (XPS)-based analysis for the assessment of photocatalytic degradation products of MB and to study the surface modifications of nanostructured ZnO thin films following the photocatalytic process, on the basis of precise determination of the surface chemical properties of our samples. In addition, the surface morphological properties of our samples were also determined by using scanning electron microscopy (SEM) as a complementary surface analytical method

2. Materials and methods

2.1. Chemicals

Si(100) substrate was purchased from Topsil. 99.95%-pure zinc Zn target was purchased from Kurt J Lesker. Isopropanol (VLSI) and acetone (VLSI) were purchased from JT Baker. The HF for the buffered solution was purchased from JT Baker. 5-N argon and 5-N oxygen were purchased from Mocart. Methylene blue (MB, Reag. Ph. Eur) was purchased from Merck. The ultrapure water was produced by a MembraPure Astacus system (MembraPure GmbH, Hennigsdorf, Germany).

2.2. Preparation of ZnO porous thin films

The nanostructured ZnO porous thin films used in the photocatalytic studies were prepared at the ŁRN - Institute of Microelectronics and Photonics, Warsaw, Poland. They were deposited at the Si(100) substrate by means of direct current (DC) reactive magnetron sputtering with post-deposition

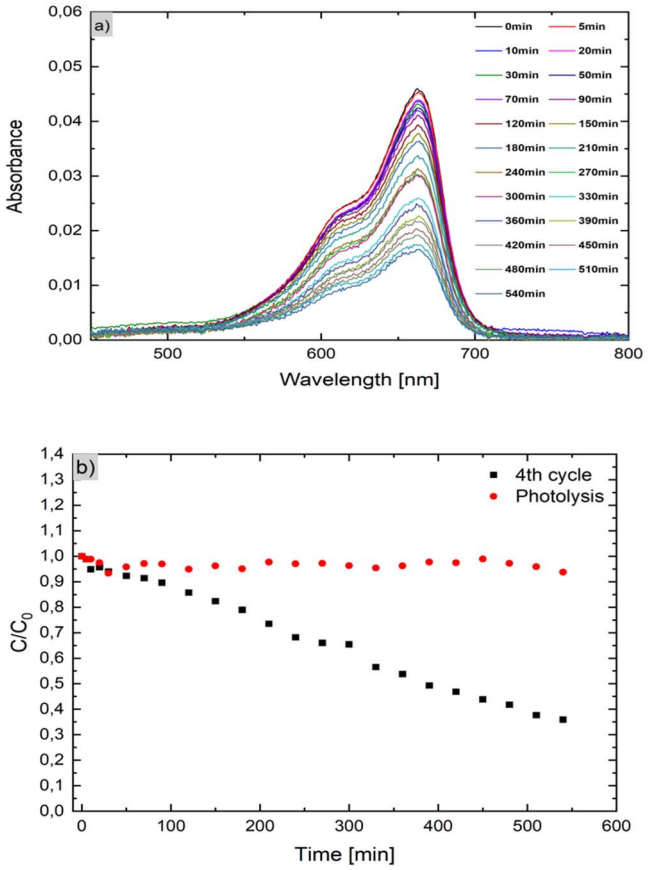

Figure 2. Temporal evolution of the UV–vis spectrum of MB (0.3 mg·l^{-1}) under UV irradiation using the nanostructured ZnO porous thin films. (a) the fourth cycle of experiments; (b) a comparison of the variation of MB concentration over time during photocatalytic and photolytic experiments.

annealing. Prior to the deposition of the nanostructured ZnO thin films, the substrate was first degreased by boiling it in isopropanol and acetone and subsequently bathed in a buffered HF solution in order to remove any native oxide.

The deposition was carried out in a high vacuum reactor (Surrey NanoSystems Gamma 1000 C, UK) using a 99.95%-pure zinc Zn target of 75 mm diameter under constant DC power of 80 W in a mixture of 5N-pure argon and oxygen flowing at 10 sccm and 1 sccm, respectively, whereas the total gas pressure during the sputtering process was equal to 0.4 Pa. The respective gas flow was controlled by mass flow controllers (MFC) and the system used a Baratron manometer in a feed-back loop with a gate throttle valve (VAT, Haag, Switzerland) for independent gas total pressure and flow control.

The base pressure in the vacuum deposition chamber prior to deposition was at the order of 10^{-5} Pa. It was pumped using a cryogenic pump (Cryo-Torr, CTI-Cryogenics, USA) placed behind the throttle valve. This step yielded a nanostructured porous Zn thin film, as reported earlier [75]. After deposition, the porous Zn thin films were oxidized to zinc oxide in a 5N-pure oxygen flow for 20 min at a temperature of 700 °C inside a rapid thermal annealing furnace (SHS 100, Mattson, USA). Other technological details concerning the fabrication of nanostructured ZnO porous thin films were previously described [76].

2.3. Characterization of ZnO nanostructured thin films

The surface morphology (grains characteristics, roughness) and surface chemistry (non-stoichiometry and contaminations) of ZnO nanostructured thin films before and after the photocatalytic activity tests were studied by using the SEM and XPS methods, respectively.

In the SEM studies, a high-resolution scanning electron microscope Carl Zeiss Auriga 60 model was used operating at 5 keV, with a lateral resolution of 2 nm. Other experimental details on SEM studies were previously described [75].

In the XPS studies, a commercial XPS spectrometer (SPECS, Berlin, Germany) was equipped, among others, with an x-ray lamp (AlK_{α}, 1486.6 eV, XR-50 model) and a concentric hemispherical analyzer (PHOIBOS-100 Model), was used. Other experimental details on XPS studies were previously described [75, 76].

2.4. Photocatalytic activity tests

The experiments on photolytic as well as photocatalytic degradation of methylene blue (MB) dye in aqueous solution (pH = 6.8) under UV light were performed for the direct comparison of their efficiency. In both experiments, 60 ml of a 0.3 mg l^{-1} MB aqueous solution were used.

The photolysis experiments were performed by irradiating the MB solution by means of 5 UV lamps (Philips, TL 8W BLB 1FM/10X25CC, $\lambda_{em,max}$ = 365 nm) with a measured irradiance ~ 1.86 mW·cm^{-2} at the level of the sample. The solution was kept under magnetic stirring during the experiment.

The photocatalytic experiments were performed in the same experimental system and conditions used for the photolysis experiments. The nanostructured ZnO thin films (1 × 1 cm) were placed horizontally in a beaker by means of golden wire support, so as to be completely submerged in the MB solution [77].

Prior to the irradiation, the system was kept in dark conditions for 30 min in order to establish the adsorption-desorption equilibrium of MB on the surface of ZnO thin films.

The changes in the UV–vis absorption spectrum of the irradiated MB solutions over time were followed via spectrophotometric measurements by making use of a Cary 100 UV–vis Spectrophotometer (Agilent, CA, USA). For these measurements, 1 ml aliquots were withdrawn at time 0 (before the start of the irradiation) and after 5, 10, 20, 30, 50, 70, 90, 120, 150, 180, 210, 240, 270, 300, 330, 360, 390, 420, 450, 480, 510, 540 min of UV irradiation.

A similar procedure was followed for the recycling experiments: after each experiment, the sample was carefully cleaned with ultrapure water, dried with compressed air, and then reused for the subsequent photocatalytic degradation of a fresh MB solution.

Table 1. Values of the rate constant k (up to 4 cycles) for the photocatalytic degradation of a 0.3 mg·l^{-1} MB solution in the presence of the ZnO thin film.

Cycle number	1st cycle	2nd cycle	3rd cycle	4th cycle
k (mol·l^{-1}·min^{-1})	$1.54{\cdot}10^{-9}$	$1.60{\cdot}10^{-9}$	$0.77{\cdot}10^{-9}$	$0.78{\cdot}10^{-9}$

The degree of degradation of MB was calculated according to the following equation:

$$\text{Degree of degradation } (\%) = \frac{c_0 - c_t}{c_0} \cdot 100, \qquad (1)$$

where c_o is the MB concentration at $t = 0$, and c_t is the MB concentration at irradiation time t.

3. Results and discussion

3.1. Photocatalytic activity of nanostructured ZnO thin films toward MB

The nanostructured ZnO porous thin films annealed at 700 °C were chosen to study the photocatalytic activity of ZnO thin films toward MB, a model dye pollutant, whose chemical structure is shown in figure S1.

Before the UV irradiation step, the ZnO thin film was submerged in a 0.3 mg·l^{-1} MB solution and kept in dark conditions for 30 min to reach the adsorption-desorption equilibrium. Subsequently, the irradiation with UV light for a total time of 540 min was performed cyclically, after rinsing the ZnO thin film in water and drying it at the end of each cycle.

The adsorption in dark conditions of MB on ZnO thin films resulted in circa 10% over 4 cycles. The UV irradiation of a 0.3 mg l^{-1} MB solution in the presence of ZnO thin film induced a decrease in the absorption band centered at 663 nm, resulting in a 64% degree of MB degradation after 540 min (figure 2).

The contribution of photolysis of MB was negligible (figure 2(b)) in the total photocatalytic degradation process, suggesting that the ZnO thin film is responsible for the photodegradation of MB.

The ZnO thin film underwent 4 photocatalytic cycles to verify its reusability (the results for the 4th cycle are shown in figure 2). After each cycle, the nanostructured ZnO porous thin film was rinsed with distilled water and subsequently air-dried.

The corresponding photocatalytic degradation curves (figure 2(b)) were analyzed to clarify the kinetics of the photocatalytic degradation of MB in the presence of ZnO porous thin film.

The fitting of the obtained data with a pseudo-first-order kinetic model was poor. This ruled out a 'diffusion-controlled' process, characterized by relatively fast surface reactions and detachment of products, yielding a negligible surface concentration of MB adsorbates, and relatively slow adsorption of MB molecules. Nevertheless, the data were better fitted using a pseudo-zero-order kinetic model, [76, 78] which describes a 'surface-reaction limited' process, in which a relatively fast adsorption equilibrium and relatively slow surface reactions occur. The following fitting equation was used:

$$c_t = c_0 - kt, \qquad (2)$$

where c_t is the MB molar concentration at time t, c_o is the MB concentration at $t = 0$ and k is the zero-order kinetic constant expressed in mol·l^{-1}·min^{-1}.

Table 1 shows the calculated values of the photocatalytic reaction rate constant for the 4 cycles. This behavior indicates that in these experimental conditions the surface of the ZnO thin film is saturated with MB molecules and that the rate-determining step is represented by the chemical reactions occurring on the surface [79].

The comparison of the obtained rate constants with the literature is extremely complex, due to the fact that most of the reports used a pseudo-first-order kinetic model to fit the data. In addition, the operational parameters (e.g. light source, irradiance, and MB initial concentration), the sample deposition techniques, the ZnO thin layer thickness, and the sample area are different, preventing a direct comparison to be performed [80–90]. Nevertheless, the fitting of the data obtained in this work with a pseudo-first-order model yields values of kinetic constants in line with the ones found in the literature (10^{-3} min^{-1}).

As shown in table 1, the value of the rate constant decreased by 50% after 4 cycles. This behavior can be ascribed to the decrease of free active sites, which can be occupied by unreacted MB and/or by its degradation products. Moreover, morphological modifications of the surface of the ZnO thin films could also occur. In order to clarify the origin of these results, a morphological and compositional analysis of the sample after the photocatalytic experiments were performed.

3.2. Surface morphology of nanostructured ZnO porous thin films

The surface morphology (grains characteristics, roughness) of the nanostructured ZnO thin films was determined via SEM measurements. Two specific images are shown in figure 3.

As shown in figure 3, the surface of nanostructured ZnO thin films presents a coral reef structure containing polycrystalline coral dendrites, as recently observed [90]. This morphology is preserved after the photocatalytic studies with no visible mesoscopic qualitative changes (figure 3(b)). A statistical analysis of the long (c) and short (d) axis lengths of the individual crystallites making up the coral structure shows that their sizes increased after the photocatalytic experiments with the median shifting from 43 to 76 nm for the longer axis

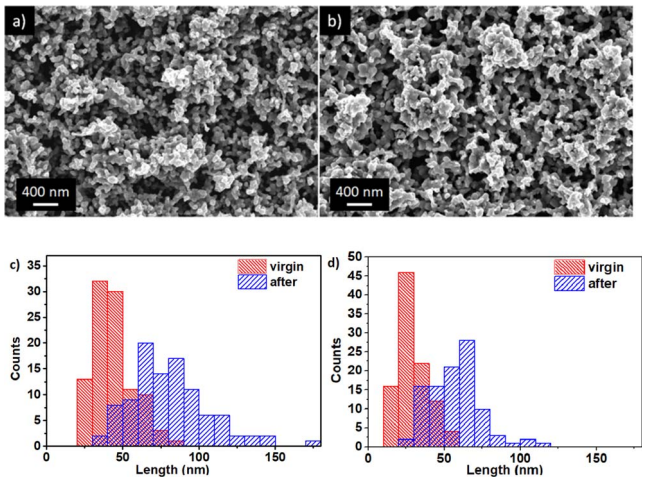

Figure 3. SEM images of the ZnO nanostructured films registered for the virgin samples (a) and for the samples after the 4th photocatalytic cycle (b), with histograms of individual nanocrystalline long (c) and short (d) axis lengths after image analysis.

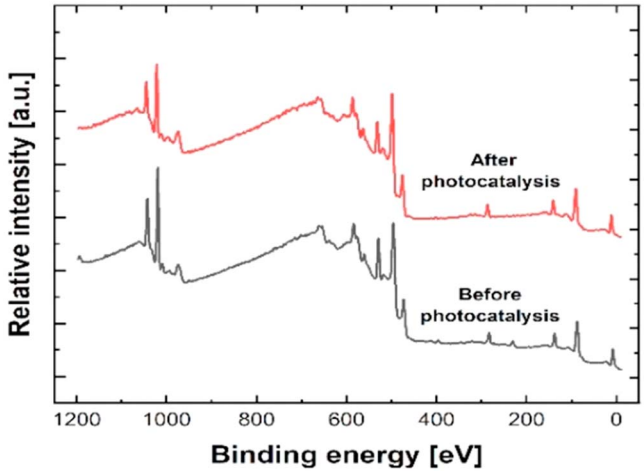

Figure 4. The XPS survey spectra of the nanostructured ZnO porous thin films before (black line) and after the 4th photocatalytic cycle (red line).

and from 28 to 58 for the shorter axis. The statistical data were calculated based on the manual determination of crystallite shape and size in the ImageJ processing program. The observed increase in crystallite size could be attributed both to (i) the presence of residual adsorbed MB or of its photodegradation by-products on the thin film surface and to (ii) the effect of UV irradiation [91].

3.3. Surface chemistry of nanostructured ZnO thin films

As mentioned above, the surface chemistry of nanostructured ZnO thin films was studied by XPS measurements, in order to assess possible non-stoichiometry and contaminations. The survey spectra combined with the specific O1s and C1s spectral lines were recorded and then analyzed.

Figure 4 shows the exemplary XPS survey spectra of the samples in the commonly used binding energy range (1200 eV) before and after the photocatalytic experiments, respectively.

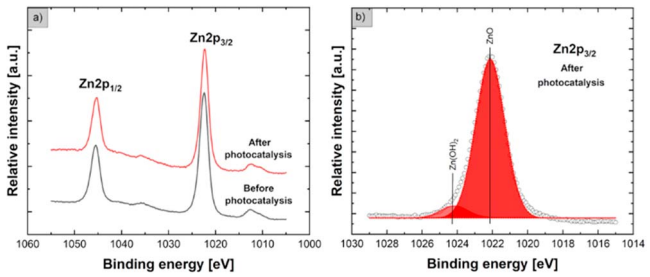

Figure 5. XPS Zn2p spectral lines of the nanostructured ZnO porous thin films before and after the photocatalytic experiment (a), together with the XPS $Zn2p_{3/2}$ spectral line for both samples after Gauss deconvolution (b).

The XPS survey spectra shown in figure 4 mainly contain the contribution from core level lines of O1s, Zn3s, Zn3p, and Zn3d, corresponding to the main elements (O and Zn) of the nanostructured ZnO thin films. Moreover, an evident contribution of C1s XPS line is also observed at 284 eV, which confirms the existence of strong C undesired contamination due to the adsorption of atmospheric CO_2. Moreover, the additional peaks related to the Auger electron emission lines at ∼570 eV, ∼500 eV, and ∼470 eV, corresponding to the Zn ($L_3M_{23}M_{45}$), Zn ($L_3M_{45}M_{45}$), and Zn ($L_2M_{45}M_{45}$) Auger electron transitions, are also present.

The XPS data analysis was performed using the commonly used analytical procedure based on the relative intensity (height) of the O1s and Zn2p core level lines (peaks), corrected by the transmission function T(E) of the CHA PHOIBOS 100, and finally after taking into account the atomic sensitivity factors (ASF) related to the height of peaks for O1s (O.66), C1s (0.25), and Zn3p (0.4), respectively. A more detailed description of the XPS data analysis was previously published [75, 76].

The analysis revealed that before the photocatalytic experiments, the relative concentration of O atoms for the nanostructured ZnO thin films was ∼ 0.25, and the relative concentration of C atoms was ∼ 0.20. Similar values were found after the photocatalytic experiments.

In addition to the procedure described above, the XPS data were analyzed using a more practical and commonly used simplified procedure to assess the surface non-stoichiometry of the nanostructured ZnO thin films by determination of the relative concentration of O and C surface atoms with respect to the Zn atoms. According to these calculations, the relative [O]/[Zn] concentration was found to be ∼ 1.4, whereas the relative [C]/[Zn] concentration was ∼ 1.2, both before and after the photocatalytic experiments.

This suggests that in both cases a significant non-stoichiometry in a surface/subsurface region of the ZnO thin films was present, which is related to the existence of various surface O atoms combined with the surface C atoms. This could be confirmed via the deconvolution procedure of XPS $Zn2p_{3/2}$, O1s and C1s spectral lines. Figure 5 shows the XPS Zn2p double lines of the nanostructured ZnO porous thin films before and after photocatalytic experiments, together with the XPS $Zn2p_{3/2}$ spectral line after Gauss deconvolution.

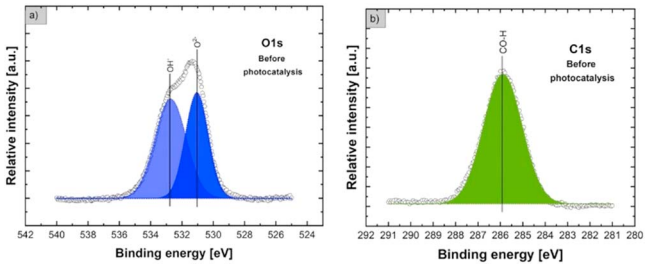

Figure 6. XPS spectra of O1s (a) and C1s (b) after Gauss deconvolution of the nanostructured ZnO porous thin films before photocatalysis.

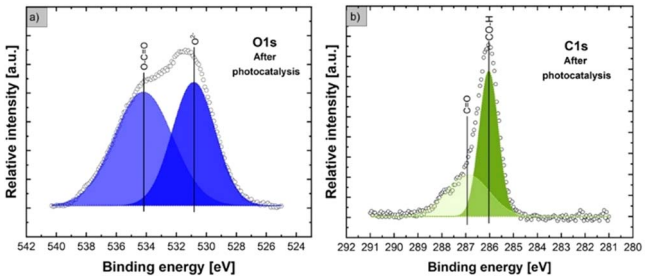

Figure 7. XPS spectra of O1s (a) and C1s (b) after Gauss deconvolution for the nanostructured ZnO porous thin films after photocatalysis.

For both cases, the XPS Zn2p lines contain two broadly resolved components at the specific binding energy of about 1045 eV and 1022 eV, respectively, related to the spin–orbit splitting of $Zn2p_{1/2}$ and $Zn2p_{3/2}$, respectively. These peaks are separated by $\sim$ 23.0 eV, which is in good agreement with available reference data [43]. This directly confirms that Zn exists mainly as Zn^{2+} corresponding to Zn atoms in the ZnO lattice [74]. However, both XPS $Zn2p_{3/2}$ lines are slightly asymmetrical. After their precise deconvolution procedure, two components were found, located at the binding energy of $\sim$1022.0 eV and $\sim$1024.0 eV, respectively, which is very clearly visible in figure 5(b). The higher one (93% of peak area), commonly observed for all ZnO samples, can be assigned to the Zn atoms in the ZnO lattice, whereas the smaller one (only 7% of peak area) to the same specific zinc hydroxide species $Zn(OH)_2$, recently observed in ZnO nanoparticles by Guo *et al* [47], in ZnO thin films as well as in the authors' XPS studies of ZnO nanowires [76]. It should be underlined that the presence of zinc hydroxide species $Zn(OH)_2$ can be expected, keeping in mind that the ZnO samples studied both before and after photocatalytic processes are usually always exposed to natural humidity conditions. Figure 6 shows the XPS spectra of O1s and C1s after Gauss deconvolution of the nanostructured ZnO thin films before photocatalysis. It is possible to observe the presence of two typical oxygen surface bonds related to hydroxide ions OH^- and the ZnO lattice oxide ions O^{2-}, at a binding energy of 531.1 eV and 532.8 eV, respectively, as well as one typical carbon surface bond related to the carbon hydroxyl group C–OH, at the binding energy 285.8 eV.

It has to be highlighted that the information on the specific surface chemical bonds related to the oxygen and carbon atoms at the surface of low dimensional ZnO nanostructures used as photocatalysts in MB degradation is still rather neglected in the available literature.

However, these bonds play an extremely important role in the photocatalytic degradation of MB, since the surface oxide ions O^{2-} can participate in the oxidation of adsorbed surface species [92] and surface oxygen hydroxide ions OH^- can capture holes to form OH radicals and can also enhance O_2 adsorption, resulting in an increased production of superoxide ions O_2^- via reduction through photogenerated electrons [68].

Interestingly, slightly different sets of surface bonds are observed after the photocatalytic experiments, as can be seen in figure 7.

As for oxygen surface bonds, the contribution of the ZnO lattice oxide ions O^{2-} is still significant after photocatalysis. Nevertheless, the surface hydroxide ions OH^- present before the photocatalysis are substituted by oxygen of the carboxyl functional O–C=O groups, at the binding energy 534.1 eV. As for the carbon surface bonds, the carbon hydroxyl group C–OH present before photocatalysis is accompanied by carbonyl functional C=O groups, at the binding energy 287.2 eV, after photocatalysis. These results suggest that carbonyl and carboxyl groups can originate from by-products of the photocatalytic degradation of MB [93]. Moreover, these adsorbed species could play a role as a specific barrier for the intra-particle diffusion of pollutant molecules on the surface of the ZnO porous thin film nanostructures, which could justify the decrease of photocatalytic activity over the irradiation cycles.

Moreover, only slight modifications of the sample morphology were observed after the photocatalytic studies with no detectable mesoscopic qualitative changes in the crystallite shape of individual crystallites of the coral structure in our porous nanostructured ZnO thin films. An increase in the crystallite size was observed after the photocatalytic experiments, with the median shifting from 43 to 76 nm for the longer axis and from 28 to 58 nm for the shorter axis. It is crucial to note that this finding is in evident contrast to the behavior of ZnO nanowires [57, 58], ZnO nanorods [59–62, 94], and hierarchical ZnO nanostructures [63–66, 95].

4. Conclusions

In this paper, the results of the photocatalytic degradation of methylene blue (MB) on ZnO nanostructured porous thin films are described with a special emphasis on the correlation with the morphology and surface chemistry of the employed nanostructured films. These films possess highly extended internal surfaces and were used as the expected most efficient photocatalyst for the MB degradation process, among the other forms of low dimensional ZnO nanomaterials reported in the literature and cited in this article. The performed photocatalytic studies showed that an MB removal of 64% was

achieved after 540 min. UV irradiation. Additionally, the reusability of these nanostructured ZnO thin films was confirmed and compared with other ZnO-based thin films reported in the literature.

The SEM studies showed that the coral dendritic structure of the pristine samples is maintained after 4 cycles of photocatalytic experiments. In addition, the XPS studies showed that the surface of the nanostructured ZnO porous thin films exhibits a slight non-stoichiometry, related to the existence of hydroxide ions OH^- . These groups can act as hole-acceptors to produce OH· radicals, which can be responsible for the generation of superoxide ions. Moreover, the superficial ZnO lattice oxide ions can also participate in the oxidation of the adsorbed MB molecules. XPS studies also revealed the presence of residual MB or its photodegradation products on the surface of the nanostructures after the photodegradation experiments, thus explaining the decrease in photocatalytic efficiency over 4 irradiation cycles.

The results of our studies confirmed that properly selected ZnO nanostructures endowed with a high surface roughness can be efficient for the photocatalytic degradation of MB. Moreover, it was confirmed that XPS is a powerful technique to better understand the surface chemistry of the photocatalyst before and after the photodegradation experiments, giving insights into the possible processes occurring during photodegradation.

Acknowledgments

A KK and MK gratefully acknowledge the national budgetary sources in the science of the Faculty of Automatic Control, Electronics, and Computer Science, Department of Cybernetics, Nanotechnology and Data Processing, Silesian University of Technology, Gliwice, Poland. The research of A KK and MK was also funded by the National Science Centre in Poland granted according to decisions DEC-2016/21/B/ST7/02244. Additionally, MK would like to acknowledge the funding of Professor Grant (GP) of the Silesian University of Technology no. 02/030/RGP19/0050. MAB acknowledges the support of the National Centre for Research and Development in the frames of the Lider V Programme through the project 'Nanocoral zinc oxide-based supercapacitors for transparent electronics (NACZO)', contract: LIDER/030/615/L-5/13/NCBR/2014. GC, NL, and MS gratefully acknowledge the financial support of the Faculty of Mechanical Science and Engineering of Technische Universität Dresden. GC, NL and MS also acknowledge the ULTIMATE project (H2020-MSCA-ITN, Grant agreement ID:813036) and DFG project 'Fabrication, characterization, and modeling of transparent semiconductor oxides' (CU 44/47–1, Project No: 424610894).

Data availability statement

The data that support the findings of this study are available upon reasonable request from the authors.

Author contributions

A KK: Formal analysis, Investigation, Writing—original draft, Writing—review & editing, Visualization. MK: Conceptualization, Methodology, Validation, Formal analysis, Resources, Writing—original draft, Writing—review & editing, Visualization, Supervision, Project administration, Funding acquisition. MAB: Methodology, Validation, Formal analysis, Writing—review & editing, Visualization. TW: Methodology, Validation, Formal analysis. NL: Conceptualization, Methodology Validation, Formal analysis, Writing—review & editing, Visualization. MS: Conceptualization, Methodology, Writing—original draft, Writing—review & editing, Visualization, Supervision, Project administration. GC: Resources, Writing—review & editing. All authors have read and agreed to the published version of the manuscript.

Conflicts of interest

The authors declare no conflict of interest.

ORCID iDs

Anna Kulis-Kapuscinska https://orcid.org/0000-0002-6719-3869
Monika Kwoka https://orcid.org/0000-0001-6197-1191
Michal Adam Borysiewicz https://orcid.org/0000-0002-7661-2412
Tomasz Wojciechowski https://orcid.org/0000-0002-6424-988X
Nadia Licciardello https://orcid.org/0000-0002-6625-2898
Massimo Sgarzi https://orcid.org/0000-0001-6938-3909
Gianaurelio Cuniberti https://orcid.org/0000-0002-6574-7848

References

[1] Hassaan M A and El Nemr A 2017 Health and environmental impacts of dyes: mini review *Am. J. Environ. Sci. Eng.* **13** 64–7
[2] Anon 1997 Color technology in the textile industry—committee RA36 color measurement test methods *American Association of Textile Chemists and Colorists* (USA: Research Triangle Park NC)
[3] Varjani S, Rakholiya P, Shindhal T, Shah A V and Ngo H H 2021 Trends in dye industry effluent treatment and recovery of value added products *J. Water Process Eng.* **39** 101734
[4] Lellis B, Fávaro-Polonio C Z, Pamphile J A and Polonio J C 2019 Effects of textile dyes on health and the environment and bioremediation potential of living organisms *Biotechnol. Res. Innov.* **3** 275–90
[5] Nidheesh P V, Zhou M and Oturan M A 2018 An overview on the removal of synthetic dyes from water by electrochemical advanced oxidation processes *Chemosphere* **197** 210–27

[6] Mittal A 2006 Adsorption kinetics of removal of a toxic dye, malachite green, from wastewater by using hen feathers *J. Hazard. Mater.* **133** 196–202

[7] Mohammed M A, Shitu A and Ibrahim A 2014 Removal of methylene blue using low cost adsorbent: a review *Res. J. Chem. Sci.* **4** 91–102

[8] Dehghani M H, Karimi B and Rajaei M S 2016 The effect of aeration on advanced coagulation, flotation and advanced oxidation processes for color removal from wastewater *J. Mol. Liq.* **223** 75–80

[9] Doke S M and Yadav G D 2014 Novelties of combustion synthesized titania ultrafiltration membrane in efficient removal of methylene blue dye from aqueous effluent *Chemosphere* **117** 760–5

[10] Ong S, Toorisaka E, Hirata M and Hano T 2005 Biodegradation of redox dye methylene blue by up-flow anaerobic sludge blanket reactor *J. Hazard. Mater.* **124** 88–94

[11] Ghoreishi S M and Haghighi R 2003 Chemical catalytic reaction and biological oxidation for treatment of non-biodegradable textile effluent *Chem. Eng. J.* **95** 163–9

[12] Buthiyappan A, Abdul Aziz A R and Wan Daud W M A 2016 Recent advances and prospects of catalytic advanced oxidation process in treating textile effluents *Rev. Chem. Eng.* **32** 1–47

[13] Hassaan M A and El Nemr A 2017 Advanced oxidation processes for textile wastewater treatment *Int. J. Photochem. Photobiol.* **1** 27–35

[14] Chan S H S, Yeong W T, Juan J C and Teh C Y 2011 Recent developments of metal oxide semiconductors as photocatalysts in advanced oxidation processes (AOPs) for treatment of dye waste-water *J. Chem. Technol. Biotechnol.* **86** 1130–58

[15] Saleh S M 2019 Metal oxide nanomaterials as photo-catalyst for dye degradation *Res. Dev. Mater. Sci.* **9** 1–8

[16] Xu C, Rangaiah G P and Zhao X S 2014 Photocatalytic degradation of methylene blue by titanium dioxide: experimental and modeling study *Ind. Eng. Chem. Res.* **53** 14641–9

[17] Che Ramli Z A, Asim N, Isahak W N R W, Emdadi Z, Ahmad-Ludin N, Yarmo M A and Sopian K 2014 Photocatalytic degradation of methylene blue under UV light irradiation on prepared carbonaceous TiO_2 *Sci. World J.* **2014** 415136

[18] Liu B, Zhao X, Terashima C, Fujishima A and Nakata K 2014 Thermodynamic and kinetic analysis of heterogeneous photocatalysis for semiconductor systems *Phys. Chem. Chem. Phys.* **16** 8751–60

[19] Wang J, Svoboda L, Němečková Z, Sgarzi M, Henych J, Licciardello N and Cuniberti G 2021 Enhanced visible-light photodegradation of fluoroquinolone-based antibiotics and *E. coli* growth inhibition using Ag–TiO_2 nanoparticles *RSC Adv.* **11** 13980–91

[20] Herrmann J-M 1999 Heterogeneous photocatalysis: fundamentals and applications to the removal of various types of aqueous pollutants *Catal. Today* **53** 115–29

[21] Pandikumar A and Jothivenkatachalam K 2019 *Photocatalytic Functional Materials for Environmental Remediation* (New York: Wiley)

[22] Zhou X, Liu G, Yu J and Fan W 2012 Surface plasmon resonance-mediated photocatalysis by noble metal-based composites under visible light *J. Mater. Chem.* **22** 21337–54

[23] Primo A, Corma A and García H 2011 Titania supported gold nanoparticles as photocatalyst *Phys. Chem. Chem. Phys.* **13** 886–910

[24] Almeida N A, Martins P M, Teixeira S, Lopes da Silva J A, Sencadas V, Kühn K, Cuniberti G, Lanceros-Mendez S and Marques P A A P 2016 TiO_2/graphene oxide immobilized in P(VDF-TrFE) electrospun membranes with enhanced visible-light-induced photocatalytic performance *J. Mater. Sci.* **51** 6974–86

[25] Silva A R, Martins P M, Teixeira S, Carabineiro S A C, Kuehn K, Cuniberti G, Alves M M, Lanceros-Mendez S and Pereira L 2016 Ciprofloxacin wastewater treated by UVA photocatalysis: contribution of irradiated TiO_2 and ZnO nanoparticles on the final toxicity as assessed by Vibrio fischeri *RSC Adv.* **6** 95494–503

[26] Teixeira S, Mora H, Blasse L-M, Martins P M, Carabineiro S A C, Lanceros-Méndez S, Kühn K and Cuniberti G 2017 Photocatalytic degradation of recalcitrant micropollutants by reusable Fe_3O_4 /SiO_2 /TiO_2 particles *J. Photochem. Photobiol. A Chem.* **345** 27–35

[27] Ulyankina A *et al* 2021 Photocatalytic degradation of ciprofloxacin in water at nano-ZnO prepared by pulse alternating current electrochemical synthesis *J. Water Process Eng.* **40** 101809

[28] Etacheri V, Seery M K, Hinder S J and Pillai S C 2011 Oxygen rich titania: a dopant free, high temperature stable, and visible-light active anatase photocatalyst *Adv. Funct. Mater.* **21** 3744–52

[29] Jang Y J, Simer C and Ohm T 2006 Comparison of zinc oxide nanoparticles and its nano-crystalline particles on the photocatalytic degradation of methylene blue *Mater. Res. Bull.* **41** 67–77

[30] Li S, Ma Z, Zhang J, Wu Y and Gong Y 2008 A comparative study of photocatalytic degradation of phenol of TiO_2 and ZnO in the presence of manganese dioxides *Catal. Today* **139** 109–12

[31] Fan H, Zhao X, Yang J, Shan X, Yang L, Zhang Y, Li X and Gao M 2012 ZnO–graphene composite for photocatalytic degradation of methylene blue dye *Catal. Commun.* **29** 29–34

[32] Senthilraja A, Subash B, Dhatshanamurthi P, Swaminathan M and Shanthi M 2015 *Spectrochim. Acta* A **138** 31–7

[33] Daneshvar N, Rasoulifard M H, Khataee A R and Hosseinzadeh F 2007 Removal of C.I. acid Orange 7 from aqueous solution by UV irradiation in the presence of ZnO nanopowder *J. Hazard. Mater.* **143** 95–101

[34] Ravishankar T N, Manjunatha K, Ramakrishnappa T, Nagaraju G, Kumar D, Sarakar S, Anandakumar B S, Chandrappa G T, Reddy V and Dupont J 2014 Comparison of the photocatalytic degradation of trypan blue by undoped and silver-doped zinc oxide nanoparticles *Mater. Sci. Semicond. Process.* **26** 7–17

[35] Jasso-Salcedo A B, Palestino G and Escobar-Barrios V A 2014 Effect of Ag, pH, and time on the preparation of Ag-functionalized zinc oxide nanoagglomerates as photocatalysts *J. Catal.* **318** 170–8

[36] Wang Y, Wang Q, Zhan X, Wang F, Safdar M and He J 2013 Visible light driven type II heterostructures and their enhanced photocatalysis properties: a review *Nanoscale* **5** 8326–39

[37] Kumari L, Li W Z, Vannoy C H, Leblanc R M and Wang D Z 2010 Zinc oxide micro- and nanoparticles: Synthesis, structure and optical properties *Mater. Res. Bull.* **45** 190–6

[38] Kumar S G and Rao K S R K 2015 Zinc oxide based photocatalysis: tailoring surface-bulk structure and related interfacial charge carrier dynamics for better environmental applications *RSC Adv.* **5** 3306–51

[39] Wang H, Xie C, Zhang W, Cai S, Yang Z and Gui Y 2007 Comparison of dye degradation efficiency using ZnO powders with various size scales *J. Hazard. Mater.* **141** 645–52
[40] Jing L, Yuan F, Hou H, Xin B, Cai W and Fu H 2005 Relationships of surface oxygen vacancies with photoluminescence and photocatalytic performance of ZnO nanoparticles *Sci. China, Ser. B Chem.* **48** 25–30
[41] Dodd A C, McKinley A J, Saunders M and Tsuzuki T 2006 Effect of particle size on the photocatalytic activity of nanoparticulate zinc oxide *J. Nanoparticle Res.* **8** 43–51
[42] Flores N M, Pal U, Galeazzi R and Sandoval A 2014 Effects of morphology, surface area, and defect content on the photocatalytic dye degradation performance of ZnO nanostructures *RSC Adv.* **4** 41099–110
[43] Raha S and Ahmaruzzaman M 2022 ZnO nanostructured materials and their potential applications: progress, challenges and perspectives *Nanoscale Adv.* **4** 1868–925
[44] Lin Y, Hu H and Hu Y H 2020 Role of ZnO morphology in its reduction and photocatalysis *Appl. Surf. Sci.* **502** 144202
[45] Ong C B, Ng L Y and Mohammad A W 2018 A review of ZnO nanoparticles as solar photocatalysts: Synthesis, mechanisms and applications *Renew. Sustain. Energy Rev.* **81** 536–51
[46] Kahsay M H, Tadesse A, RamaDevi D, Belachew N and Basavaiah K 2019 Green synthesis of zinc oxide nanostructures and investigation of their photocatalytic and bactericidal applications *RSC Adv.* **9** 36967–81
[47] Guo M Y, Fung M K, Fang F, Chen X Y, Ng A M C, Djurišić A B and Chan W K 2011 ZnO and TiO2 1D nanostructures for photocatalytic applications *J. Alloys Compd.* **509** 1328–32
[48] Xia Y, Wang J, Chen R, Zhou D and Xiang L 2016 A Review on the Fabrication of Hierarchical ZnO Nanostructures for Photocatalysis Application *Crystals* **6** 148
[49] Mohd Adnan M A, Julkapli N M and Abd Hamid S B 2016 Review on ZnO hybrid photocatalyst: impact on photocatalytic activities of water pollutant degradation *Rev. Inorg. Chem.* **36** 77–104
[50] Verma H K, Vij M and Maurya K K 2020 Synthesis, characterization and sun light-driven photocatalytic activity of zinc oxide nanostructures *J. Nanosci. Nanotechnol.* **20** 3683–92
[51] Di Mauro A, Fragalà M E, Privitera V and Impellizzeri G 2017 ZnO for application in photocatalysis: from thin films to nanostructures *Mater. Sci. Semicond. Process.* **69** 44–51
[52] Ankamwar B G, Kamble V B, Annsi J I, Sarma L S and Mahajan C M 2017 Solar photocatalytic degradation of methylene blue by ZnO nanoparticles *J. Nanosci. Nanotechnol.* **17** 1185–92
[53] Hanif M, Lee I, Akter J, Islam M, Zahid A, Sapkota K and Hahn J 2019 Enhanced photocatalytic and antibacterial performance of ZnO nanoparticles prepared by an efficient thermolysis method *Catalysts* **9** 608
[54] Balcha A, Yadav O P and Dey T 2016 Photocatalytic degradation of methylene blue dye by zinc oxide nanoparticles obtained from precipitation and sol-gel methods *Environ. Sci. Pollut. Res.* **23** 25485–93
[55] Mandal T K, Malhotra S P K and Singh R K 2018 Photocatalytic degradation of methylene blue in presence of ZnO nanopowders synthesized through a green synthesis metods *Rom. J. Mater.* **48** 32–8
[56] Li Z and Gao W 2004 ZnO thin films with DC and RF reactive sputtering *Mater. Lett.* **58** 1363–70
[57] Alfaro Cruz M R, Ceballos-Sanchez O, Luévano-Hipólito E and Torres-Martínez L M 2018 ZnO thin films deposited by RF magnetron sputtering: Effects of the annealing and atmosphere conditions on the photocatalytic hydrogen production *Int. J. Hydrogen Energy* **43** 10301–10
[58] Prasada Rao T, Santhosh Kumar M C, Safarulla A, Ganesan V, Barman S R and Sanjeeviraja C 2010 Physical properties of ZnO thin films deposited at various substrate temperatures using spray pyrolysis *Phys. B Condens. Matter* **405** 2226–31
[59] Komaraiah D, Radha E, Vijayakumar Y, Sivakumar J, Reddy M V R and Sayanna R 2016 Optical, structural and morphological properties of photocatalytic ZnO thin films deposited by pray pyrolysis technique *Mod. Res. Catal.* **5** 130–46
[60] Lv J, Gong W, Huang K, Zhu J, Meng F, Song X and Sun Z 2011 Effect of annealing temperature on photocatalytic activity of ZnO thin films prepared by sol–gel method *Superlattices Microstruct.* **50** 98–106
[61] Shankar S, Saroja M, Venkatachalam M and Parthasarathy G 2017 Photocatalytic degradation of methylene blue dye using ZnO thin films *Int. J. Chem. Concepts* **3** 180–8
[62] Horzum N, Hilal M E and Isık T 2018 Enhanced bactericidal and photocatalytic activities of ZnO nanostructures by changing the cooling route *New J. Chem.* **42** 11831–8
[63] Smazna D, Shree S, Polonskyi O, Lamaka S, Baum M, Zheludkevich M, Faupel F, Adelung R and Mishra Y K 2019 Mutual interplay of ZnO micro- and nanowires and methylene blue during cyclic photocatalysis process *J. Environ. Chem. Eng.* **7** 103016
[64] Azam A and Babkair S 2014 Low-temperature growth of well-aligned zinc oxide nanorod arrays on silicon substrate and their photocatalytic application *Int. J. Nanomedicine* **9** 2109–15
[65] Bourfaa F, Boutelala A, Aida M S, Attaf N and Ocak Y S 2020 Influence of seed layer surface position on morphology and photocatalysis efficiency of ZnO nanorods and nanoflowers *J. Nanomater.* **2020** 1–9
[66] Rosa A P P D, Cavalcante R P, Silva T F D, Gozzi F, Byrne C, McGlynn E, Casagrande G A, Oliveira S C D and Junior A M 2020 Photoelectrocatalytic degradation of methylene blue using ZnO nanorods fabricated on silicon substrates *J. Nanosci. Nanotechnol.* **20** 1177–88
[67] Kuriakose S, Bhardwaj N, Singh J, Satpati B and Mohapatra S 2013 Structural, optical and photocatalytic properties of flower-like ZnO nanostructures prepared by a facile wet chemical method *Beilstein J. Nanotechnol.* **4** 763–70
[68] Kuriakose S 2015 Effects of solvent on structural, optical and photocatalytic properties Of ZnO nanostructures *Adv. Mater. Lett.* **6** 1104–10
[69] Hong Y, Tian C, Jiang B, Wu A, Zhang Q, Tian G and Fu H 2013 Facile synthesis of sheet-like ZnO assembly composed of small ZnO particles for highly efficient photocatalysis *J. Mater. Chem. A* **1** 5700–8
[70] Lucic Lavcevic M and Penava A 2017 ZnO nanostructured photocatalysts for water treatment applications *Croat. J. Food Sci. Technol.* **9** 192–7
[71] Zhang F 2017 Electrodeposition of ZnO Film With Enhanced Photocatalytic Activity Towards Methylene Blue Degradation *Int. J. Electrochem. Sci.* **12** 3756–64
[72] Silva I M P, Byzynski G, Ribeiro C and Longo E 2016 Different dye degradation mechanisms for ZnO and ZnO doped with N (ZnO:N) *J. Mol. Catal. A: Chem.* **417** 89–100
[73] Luque-Morales P A, Lopez-Peraza A, Nava-Olivas O J, Amaya-Parra G, Baez-Lopez Y A, Orozco-Carmona V M, Garrafa-Galvez H E and Chinchillas-Chinchillas M D J 2021 ZnO semiconductor nanoparticles and their application in photocatalytic degradation of various organic dyes *Materials* **14** 7537
[74] Jagadish C and Pearton S 2006 *Zinc Oxide Bulk, Thin Films and Nanostructures* (Amsterdam: Elsevier Science)
[75] Masłyk M, Borysiewicz M A, Wzorek M, Wojciechowski T, Kwoka M and Kamińska E 2016 Influence of absolute argon and oxygen flow values at a constant ratio on the growth of

Zn/ZnO nanostructures obtained by DC reactive magnetron sputtering *Appl. Surf. Sci.* **389** 287–93
[76] Kwoka M, Lyson-Sypien B, Kulis A, Maslyk M, Borysiewicz M, Kaminska E and Szuber J 2018 Surface properties of nanostructured, porous ZnO thin films prepared by direct current reactive magnetron sputtering *Materials.* **11** 131
[77] Pennisi F M, Pellegrino A L, Licciardello N, Mezzalira C, Sgarzi M, Speghini A, Malandrino G and Cuniberti G 2022 Synthesis, characterization and photocatalytic properties of nanostructured lanthanide doped β-$NaYF_4/TiO_2$ composite films *Sci. Rep.* **12** 13748
[78] Mills A, Sheik M, O'Rourke C and McFarlane M 2009 Adsorption and photocatalysed destruction of cationic and anionic dyes on mesoporous titania films: reactions at the air–solid interface *Appl. Catal. B Environ.* **89** 189–95
[79] Ohtani B 2010 Photocatalysis A to Z—What we know and what we do not know in a scientific sense *J. Photochem. Photobiol. C Photochem. Rev.* **11** 157–78
[80] Pauporté T and Rathouský J 2007 Electrodeposited mesoporous ZnO thin films as efficient photocatalysts for the degradation of Dye pollutants *J. Phys. Chem. C* **111** 7639–44
[81] Ali A M, Emanuelsson E A C and Patterson D A 2010 Photocatalysis with nanostructured zinc oxide thin films: the relationship between morphology and photocatalytic activity under oxygen limited and oxygen rich conditions and evidence for a Mars Van Krevelen mechanism *Appl. Catal. B Environ.* **97** 168–81
[82] Dash P, Manna A, Mishra N C and Varma S 2019 Synthesis and characterization of aligned ZnO nanorods for visible light photocatalysis *Phys. E Low-dimens. Syst. Nanostructures* **107** 38–46
[83] Park K-H, Han G D, Kim B J, Kang E H, Park J S, Shim J H and Park H-D 2019 Effects of atomic layer deposition conditions on the formation of thin ZnO films and their photocatalytic characteristics *Ceram. Int.* **45** 18823–30
[84] Rivera Z R, Alvarez A M and Amador M 2019 *2019 16th Int. Conf. on Electrical Engineering, Computing Science and Automatic Control (CCE) (Mexico)* pp 1–6
[85] Ennaceri H, Wang L, Erfurt D, Riedel W, Mangalgiri G, Khaldoun A, El Kenz A, Benyoussef A and Ennaoui A 2016 Water-resistant surfaces using zinc oxide structured nanorod arrays with switchable wetting property *Surf. Coatings Technol.* **299** 169–76
[86] Frunza L, Diamandescu L, Zgura I, Frunza S, Ganea C P, Negrila cc, Enculescu M and Birzu M 2018 Photocatalytic activity of wool fabrics deposited at low temperature with ZnO or TiO_2 nanoparticles: methylene blue degradation as a test reaction *Catal. Today* **306** 251–9
[87] Talebian N and Nilforoushan M R 2010 Comparative study of the structural, optical and photocatalytic properties of semiconductor metal oxides toward degradation of methylene blue *Thin Solid Films* **518** 2210–5
[88] Yi X Y, Ma C Y, Yuan F, Wang N, Qin F W, Hu B C and Zhang Q Y 2017 Structural, morphological, photoluminescence and photocatalytic properties of Gd-doped ZnO films *Thin Solid Films* **636** 339–45
[89] Miyauchi M, Nakajima A, Watanabe T and Hashimoto K 2002 Photocatalysis and photoinduced hydrophilicity of various metal oxide thin films *Chem. Mater.* **14** 2812–6
[90] Sapkal R T, Shinde S S, Waghmode T R, Govindwar S P, Rajpure K Y and Bhosale C H 2012 Photo-corrosion inhibition and photoactivity enhancement with tailored zinc oxide thin films *J. Photochem. Photobiol. B Biol.* **110** 15–21
[91] Soleimanpour A M, Hou Y and Jayatissa A H 2011 The effect of UV irradiation on nanocrysatlline zinc oxide thin films related to gas sensing characteristics *Appl. Surf. Sci.* **257** 5398–402
[92] Borysiewicz M A, Wzorek M, Wojciechowski T, Wojtowicz T, Kamińska E and Piotrowska A 2014 Photoluminescence of nanocoral ZnO films *J. Lumin.* **147** 367–71
[93] Ali A M, Emanuelsson E A C and Patterson D A 2011 Conventional versus lattice photocatalysed reactions: implications of the lattice oxygen participation in the liquid phase photocatalytic oxidation with nanostructured ZnO thin films on reaction products and mechanism at both 254nm and 340nm *Appl. Catal. B Environ.* **106** 323–36
[94] Bandekar G, Rajurkar N S, Mulla I S, Mulik U P, Amalnerkar D P and Adhyapak P V 2014 Synthesis, characterization and photocatalytic activity of PVP stabilized ZnO and modified ZnO nanostructures *Appl. Nanosci.* **4** 304–8
[95] Zeferino R S, Ramón J A R, Reyes M E, de A, González R S and Pal U 2016 Large scale synthesis of ZnO nanostructures of different morphologies through solvent-free mechanochemical synthesis and their application in photocatalytic dye degradation *Am. J. Eng. Appl. Sci.* **9** 41–52